Structural transformation of Ag_3PO_4 and Ag_3PO_4/TiO_2 induced by visible light and Cl^- ions: its impact on their photocatalytic, antimicrobial, and antifungal performance

KATARÍNA BAĎUROVÁ[1], MARTIN MOTOLA[*2], ADRIANA JANCZURA[3], TOMÁŠ ROCH[4], LEONID SATRAPINSKYY[4], JÁN GREGUŠ[4], EWA DWORNICZEK[3], GUSTAV PLESCH[1]

[1]*Department of Inorganic Chemistry, Faculty of Natural Sciences, Comenius University, Ilkovicova 6, 842 15 Bratislava, Slovakia*

[2]*Center of Materials and Nanotechnologies, Faculty of Chemical Technology, University of Pardubice, Nam. Cs. Legii 565, 530 02 Pardubice, Czech Republic*

[3]*Department of Microbiology, Faculty of Medicine Wroclaw Medical University, 50 368 Wroclaw, Poland*

[4]*Department of Experimental Physics, Faculty of Mathematics, Physics and Informatics, Comenius University, Mlynska Dolina, 842 48 Bratislava, Slovakia*

[*]Corresponding author, e-mail: martin.motola@upce.cz

Abstract

In this work, synthesis of Ag_3PO_4 and its composite with TiO_2 (Ag_3PO_4/TiO_2) towards study of two phenomena naturally occurring in Ag_3PO_4 is reported. Specifically, a visible light-driven (i.e., photocorrosion) and chloride ion-driven transformation of Ag_3PO_4 to $AgCl$ in chloride-free and chloride-present aqueous solution. A deeper insight on this transformation *via* study of their structural and morphological changes using X-ray diffractometry (XRD), scanning electron microscopy (SEM), energy-dispersive X-ray spectroscopy (EDS) is performed. Substantial amount of $AgCl$ is detected in both Ag_3PO_4 based materials after visible light irradiation in chloride-present environment. This led to increase in optical band gap of Ag_3PO_4 and Ag_3PO_4/TiO_2 from 2.52 eV to 2.99 eV and 2.48 eV to 3.02 eV, respectively. Impact of these structural changes in Ag_3PO_4 and Ag_3PO_4/TiO_2 on their photocatalytic activity is evaluated from the photoinduced catalytic, antibacterial, and antifungal performance under visible light irradiation. The photocatalytic activity of pristine and photocorroded Ag_3PO_4 is increased by ~10 times compared to that of pristine and photocorroded Ag_3PO_4/TiO_2. Photocorroded Ag_3PO_4 and Ag_3PO_4/TiO_2 possess minor antibacterial and antifungal activities (cell survival ~90 %). Whereas using pristine Ag_3PO_4 and Ag_3PO_4/TiO_2 the cell survival is reduced by 100 % after 60 and 120 min, respectively.

Keywords: Photocatalysis, Antimicrobial, Antifungal, Photocorrosion, Ag_3PO_4, TiO_2, $AgCl$

Introduction

Contamination of freshwater systems by organic pollutants and microorganisms from industrial effluent, agricultural runoff, and wastewater is a serious threat to the environment (Lapworth et al., 2012; Schwarzenbach et al., 2006). With increasing resistance of microorganisms to antibiotics and disinfectants, undoubtedly affecting the overall public health, development of photoinduced catalytic and antibacterial materials has received significant attention (Chatterjee et al., 2005; Wu et al., 2019). Photocatalysis is based on the incident light absorption, generation of electron/hole (e^-/h^+) pairs, and subsequent formation of reactive oxygen species (ROS) with high oxidizing power (Hoffmann et al., 1995). It is reported that in most cases ROS are responsible for decomposition of environmental pollutants (Houas et al., 2001; Zhao et al., 2004) and are also capable of damaging biomolecules and regulate cell death (Du et al., 2004; Overmyer et al., 2003). Nowadays, TiO_2 is one of the most commonly used photocatalyst

(Malato et al., 2009; Motola et al., 2019; Motola et al., 2017; Schneider et al., 2014; Sopha et al., 2020). However, since TiO_2 is a n-type semiconductor with a band gap energy of ~3.2 eV for anatase phase (the most photocatalytically active phase of TiO_2), a significant photoresponse is generated by UV light (λ < 390 nm). This limits its practical application. The photocatalytic activity of TiO_2 can be enhanced using reasonable methods (e.g., by doping, by additional coating or decorating, etc.) to improve charge transfer and lower recombination rate of e^-/h^+ pairs in TiO_2 (Beketova et al., 2020; Krbal et al., 2019; Motola et al., 2019; Motola et al., 2018; Wetchakun et al., 2019). Another option is to look for photocatalysts with lower band gap compared to TiO_2, which work efficiently in VIS light e.g., $BiVO_4$ (Monfort et al, 2018) or Ag_3PO_4 (Baďurová et al., 2017; Zhang et al., 2015).

Recently much effort has been devoted to study of Ag_3PO_4, which is a highly promising photocatalytic material with an indirect band gap of ~2.36 eV and high quantum efficiency (up to 90 % at 420 nm) (Hewer et al., 2014; Kumar ete al., 2014). Enhanced photoinduced catalytic (Hewer et al., 2014; Kumar et al., 2014) and antibacterial (Hong et al., 2016; Piccirillo et al., 2015) activity of Ag_3PO_4 compared to TiO_2 is reported. In particular, the antimicrobial activity of Ag_3PO_4 is widely studied, mainly because Ag and some of its compounds are used as an efficient disinfectants for thousands of years (Silvestry-Rodriguez et al., 2007). The antibacterial activity of Ag_3PO_4 proceeds on its surface *via* a following three-step mechanism (Lee et al., 2005; Liu et al., 2012; Markowska et al., 2013): 1) Ag_3PO_4 ionizes partially in aqueous solutions to release Ag^+ ions with stable and controlled rate. Ag^+ directly kills bacteria by hindering the deoxyribonucleic acid (DNA) replication and by inhibiting the expression of ribosomal proteins and enzymes for adenosine triphosphate (ATP) hydrolysis; 2) under visible (VIS) light irradiation, Ag_3PO_4 generates e^-/h^+ pairs with low recombination rate. The generated e^-/h^+ pairs ultimately produce ROS which are responsible for oxidative damage of microbial cells and photoinduced disinfectant properties; 3) Simultaneously, PO_4^{3-} ions are involved in the interconversion cycle of ATP and adenosine diphosphate (ADP). First, one of the phosphate molecules reduces the ATP from three-to-two phosphate forming ADP and PO_4^{3-} ions. Second, the formation of ATP takes place with ADP and PO_4^{3-} ions. The PO_4^{3-} ions affects the formation of ATP causing disturbance in the interconversion cycle. This leads to the lagging of growth and proliferation of bacteria.

Despite the promising photocatalytic and photoinduced antibacterial properties of Ag_3PO_4, the material suffers from a poor photostability. This results in a fast photoreduction into metallic Ag (Yang et al., 2015). To overcome this drawback, Ag_3PO_4 composites with various materials such as Ag/Ag_3PO_4 (Teng et al., 2012), AgX/Ag_3PO_4 (Bi et al., 2011; Teng et

al., 2012; Wang et al., 2013), TiO_2/Ag_3PO_4 (Yang et al., 2015; Zhao et al., 2014), SnO_2/Ag_3PO_4 (Zhang et al., 2012), carbon quantum dots/Ag_3PO_4 (Zhang et al., 2012), and graphene oxide/Ag_3PO_4 (Liang et al., 2012) are suggested. Moreover, the photocatalytic and antibacterial properties of Ag_3PO_4 composite is promising. Enhanced photocatalytic properties of such Ag_3PO_4 composite is *due* to the relative position of the valence and the conduction band of Ag_3PO_4 and the specific compound in Ag_3PO_4 composite which facilitate the interfacial charge transfer and suppress the e^-/h^+ recombination rate in material. Liu et al. (Liu et al., 2017) reported that TiO_2 incorporated into Ag_3PO_4 enhances VIS light-driven photocatalytic activity with promising cycling stability and inhibits photocorrosion of Ag_3PO_4. By integrating Ag_3PO_4 with TiO_2, the e^-/h^+ separation is facilitated (Serpone et al., 1995; Yao et al., 2012; Yi et al., 2010). Thus, the photocatalytic activity of Ag_3PO_4/TiO_2 is enhanced *due* to improved charge carrier separation. The position of the conduction band (-0.3 eV vs. NHE) and the valence band (+2.7 eV vs. NHE) of TiO_2 is more negative compared those of Ag_3PO_4 (conduction band = +0.45 eV vs. NHE; valence band = 2.9 eV vs. NHE) (Serpone et al., 1995; Yao et al., 2012; Yi et al., 2010). Therefore, under VIS light irradiation, photogenerated h^+ in Ag_3PO_4 are transfered to TiO_2, whereas photogenerated e^- migrate to the surface of Ag_3PO_4. This separation of e^- (trapped in Ag_3PO_4) and h^+ (trapped in TiO_2) prevents their recombination, leading to a higher photocatalytic activity of Ag_3PO_4/TiO_2 composite. However, not all published results are satisfactory regarding the enhanced photocatalytic activity of Ag_3PO_4/TiO_2 compared to pristine Ag_3PO_4 (Baďurová et al., 2017). Moreover, photoinduced antibacterial activity of Ag_3PO_4 is frequently evaluated by a certain bacterial concentration adjusted by serial dilution of sterilized NaCl solution (Roy et al., 2012), liquid nutrient medium (Sadowski et al., 2015), phosphate buffered saline (PBS) solution (Liu et al., 2012), or in Luria-Bertani culture medium (Roy et al., 2012). As reported by Hong et al. (Hong et al., 2016), a transformation of Ag_3PO_4 to AgCl in the presence of Cl^- ions in Ag_3PO_4/hydroxyapatite composite occurs. As AgCl itself possess photoinduced catalytic (Dong et al., 2012; Hu et al., 2006; Rehan et al., 2018) and antibacterial (Chen et al., 2015; Kang et al., 2016) activity, Hong et al. refers to it as a dual antibacterial effect. To the best of our knowledge, a study on the photoinduced catalytic and antibacterial activity of Ag_3PO_4 and Ag_3PO_4/TiO_2 composite in saline (0.80 % aqueous NaCl) along with the characterization of the structural changes of Ag_3PO_4 proceeding during these measurements is not yet reported.

In this work, an insight on the structural and morphological changes of Ag_3PO_4 and Ag_3PO_4/TiO_2 composite in chloride-free aqueous solution and in saline under VIS light irradiation is presented. The VIS light-driven and chloride ion-driven transformation of Ag_3PO_4

125 to AgCl is investigated. Influence of these two phenomena on VIS light-driven photocatalytic
126 activity (using a model organic dye) and on *in vitro* photoinduced antibacterial and antifungal
127 activity using *Stenotrophomonas maltophilia* and *Candida albicans* is discussed.

128

Experimental

130

Synthesis and characterization

132

133 For this study, two batches of Ag_3PO_4 based materials are prepared: 1) Ag_3PO_4 (AGP) and its
134 composite with TiO_2 (AGP/P25) and 2) their photocorroded counterparts AGP-pc and
135 AGP/P25-pc. Pristine AGP and AGP/P25 are prepared as previously reported (Baďurová et
136 al., 2017). Briefly, 0.75 M aqueous solution of $Na_3PO_4 \cdot 12H_2O$ is added dropwise under
137 vigorous magnetic stirring into 0.25 M aqueous solution of $AgNO_3$ followed by 12 h stirring
138 in dark (to prevent the photocorrosion of the material) to obtain AGP. The AGP/P25 is prepared
139 by an impregnation method. First, TiO_2 powder (Aeroxide P25 Degussa) is dispersed in
140 deionized water in an ultrasonic bath. Second, the solution of $AgNO_3$ (0.25 M) is added to
141 TiO_2 and the suspension is stirred for 2 h. Finally, the $Na_3PO_4 \cdot 12H_2O$ solution is added into
142 the suspension and stirred for another 2 h on a magnetic stirrer and 1 h in an ultrasonic bath,
143 respectively. Afterwards, both materials are washed several times with deionized water and
144 dried at 80 °C for 24 h. To obtain photocorroded material (AGP-pc and AGP/P25-pc),
145 irradiation under xenon lamp ($\lambda = 290 - 400$ nm) for 30 min in a water suspension is performed.
146 For the purpose of comparison a partial-to-full Ag_3PO_4 to AgCl materials are prepared; AGP
147 and AGP/P25 are immersed in a saline solution (0.80 %) and are irradiated by VIS light for 30
148 min to obtain such transformed material, yielding t-AGP and t-AGP/P25, respectively.

149 Structure and morphology of all Ag_3PO_4 based materials is investigated by X-ray
150 diffraction (XRD) using PANalytical XPert PRO MRD diffractometer (Cu-Kα radiation,
151 Bragg-Brentano mode, 20 – 70° 2θ), scanning electron microscopy (SEM) with backscattering
152 electron (BSE) method, and energy dispersive X-ray spectroscopy (EDS) on FIB Lyra 3 Tescan
153 microscope. Quantitative Rietveld analysis of XRD data (SW program MAUD) is used to
154 quantify the content of metallic Ag in all materials.

155 Diffuse reflectance spectra (DRS) of prepared Ag_3PO_4 based materials are recorded on
156 Ocean Optic USB650UV spectrometer equipped with an optical fiber (R200-7-SR) using a
157 deuterium lamp and tungsten halogen lamp as the light sources in the wavelength range 300 –
158 800 nm.

Photoinduced catalytic, antimicrobial and antifungal measurements

The photocatalytic activity is investigated by monitoring the photodegradation of methylene blue (MB with initial concentration 10^{-5} M) under constant stirring and bubbling with air in a self-constructed apparatus (Michal et al., 2014) using a metal-halogenide lamp (HQI TS – OSRAM 400 W, λ_{max} = 525 nm) with the spectral distribution characteristics and intensity comparable to the natural sunlight. As solvent, 0.80 % aqueous NaCl is used. Prior to all measurements, the 0.1 g of photocatalyst is placed for 30 min in 100 mL of the dye solution in the dark to achieve adsorption/desorption equilibrium. The decrease in dye concentration is estimated from the absorbance of the solution measured at 664 nm using a UV-VIS spectrophotometer (Jasco V-530).

For antimicrobial and antifungal experiments, clinical strains of *Stenotrophomonas maltophilia* 5778p and *Candida albicans* 266 are used. The overnight cultures are centrifugated and diluted in a 0.80 % aqueous NaCl to a concentration of 10^8 CFU/mL (colony forming unit per milliliter) for *S.maltophilia* and 10^6 CFU/mL for *C. albicans*, as determined from optical density measurements (OD_{600}). Then 1 mL of the bacterial/fungal culture is mixed with the powder's suspensions in a glass dish to give a final concentration of 48 µg/mL (no cytotoxic activity). Control microbial cultures exposed to light without powders are also set up. To prevent settling of the powders, the dishes are placed on a plate with continuous stirring. At each time point of irradiation (at 30 min, 60 min, 90 min, and 120 min using Xenon lamp 50mW/cm^2), 100 µl/mL of the suspension is removed, diluted, and inoculated (50 µl) onto nutrient agar plates. Following incubation, (24 - 48 h at 37 °C for bacteria and 48 - 72 h at 28-30 °C for fungi) original colony count (CFU/mL) is determined. All experiments are performed three times and at least in triplicate.

Results and discussion

Characterization of Ag₃PO₄ based materials

XRD patterns of all Ag₃PO₄ based materials are shown in Fig. 1. All diffractions in the XRD pattern of AGP (Fig. 1a) are attributed to Ag₃PO₄ adopting the cubic structure with space group $P\bar{4}3n$ (ICDD 01-070-0702). For photocatalytic applications, the cubic Ag₃PO₄ is considered to

be superior to those of rhombic dodecahedral and other structural types of Ag_3PO_4 (Bi et al., 2012; Yi et al., 2010) although there are reports which state *vice versa* (Bi et al., 2011). Nevertheless, acknowledged photocatalytically active cubic structure of Ag_3PO_4 is achieved during the synthesis. Similar diffractions of the cubic Ag_3PO_4 are detected for AGP/P25 (Fig. 1b). In case of AGP/P25, additional strong diffraction of (101) tetragonal anatase TiO_2 with space group $I4_1/amd$ (ICDD 01-084-1285) at $2\theta = \sim25.3°$ clearly demonstrates the successful preparation of Ag_3PO_4/TiO_2 composite. To study the VIS light- and the chloride ion-driven transformation impact on the structural changes of Ag_3PO_4 based materials proceeded throughout photocatalytic experiments, the material is irradiated for 2 h under VIS light in saline. Every 30 min, the XRD is re-measured to monitor the proceeded structural changes. 2 h irradiation time is used *due* to similar conditions used for photoinduced antimicrobial and antifungal activity tests (which are discussed in the next chapter). A significant decrease in the intensity of Ag_3PO_4 diffractions and several new diffractions appear in AGP (Fig. 1a) after 30 min VIS light irradiation. The newly detected diffractions are attributed to AgCl possessing halite crystal structure with space group $Fm\overline{3}m$ (IDCC 01-085-1355). Hong et al. (Hong et al., 2016) previously described this phenomenon, which indicates chloride ion-driven partial transformation of Ag_3PO_4 to AgCl in chloride-based solution during VIS light irradiation. AgCl is formed as a result of a reaction between Ag^+ (released from irradiated Ag_3PO_4) and Cl^- (from saline). After 2 h VIS light irradiation, the chloride ion-driven transformation of Ag_3PO_4 to AgCl in AGP is almost fulfilled. This is clearly seen from the changes in the diffraction intensity of Ag_3PO_4. In particular, the (210) diffraction intensity of Ag_3PO_4 significantly decreased with longer irradiation times. Simultaneously, the diffractions of AgCl are more pronounced with longer irradiation times. The chloride ion-driven transformation of Ag_3PO_4 to AgCl is observed also in AGP/P25 (Fig. 1b). However, the most intense (210) diffraction of Ag_3PO_4 is clearly visible after 2 h irradiation. This indicates that lower amount of Ag_3PO_4 did suffer the transformation to AgCl. The difference in the transformation of Ag_3PO_4 to AgCl between AGP and AGP/P25 is described as follows. The transformation of Ag_3PO_4 to AgCl proceeds on the interface between Ag_3PO_4 (its exposed surface) and the incident VIS light in the presence of Cl^-. In AGP, which contains only pure Ag_3PO_4, the transformation occurs on every particle exposed to its surroundings. On the other hand, in AGP/P25, additional TiO_2 nanoparticles attached on parts of the surface of Ag_3PO_4 blocks the direct contact of Ag_3PO_4 with surrounding Cl^- and shades the incident VIS light. Thus, by creating a physical barrier on Ag_3PO_4 by TiO_2, the transformation of Ag_3PO_4 to AgCl in AGP/P25 is significantly lower compared to that in AGP. This shading of Ag_3PO_4 by TiO_2 nanoparticles is clearly visible on SEM (Fig. 2b).

Further, the quantitative Rietveld analysis of the XRD data is performed to quantify the content of metallic Ag after 120 min irradiation in saline in all Ag_3PO_4 based materials. The average w% of Ag in AGP, AGP/P25, AGP-pc and AGP/P25-pc is 2 %, 2.5 %, 1.5 % and 1.3 %, respectively.
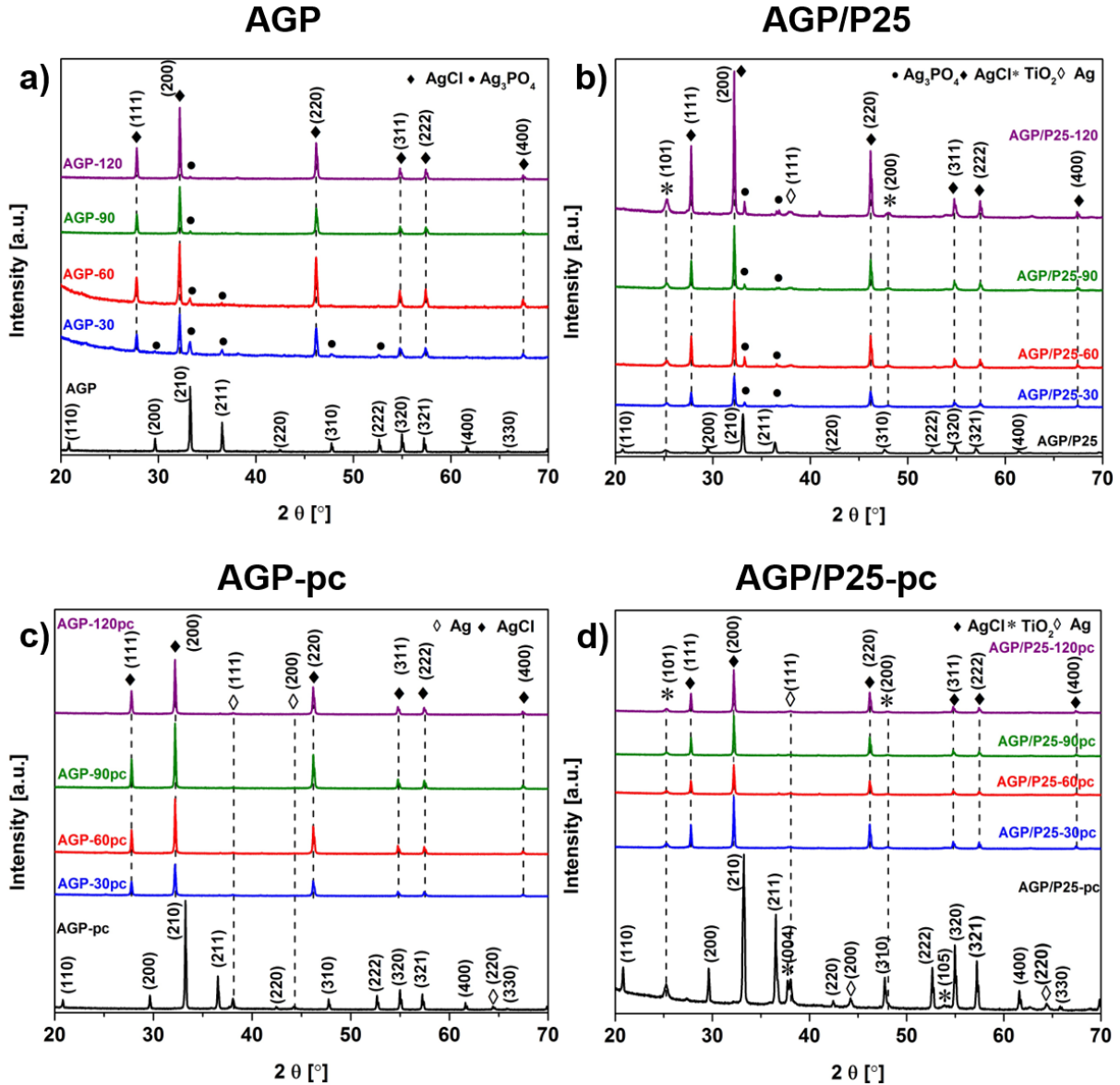
Fig. 1. XRD patterns of a) Ag_3PO_4 (AGP); b) Ag_3PO_4/TiO_2 (AGP/P25) and their photocorroded counterparts c) AGP-pc; d) AGP/P25-pc. The number (30, 60, 90, 120) specifies the irradiation time in minutes under VIS light irradiation in saline.

Ag_3PO_4 based materials are well known for their high photosensitivity (Yang et al., 2015; Zhao et al., 2014). Therefore, it is crucial to monitor their structural changes caused by light irradiation. For this purpose, photocorroded Ag_3PO_4 based materials are also investigated. Prior to any other experiments, AGP and AGP/P25 are irradiated under VIS light for 30 min to

obtain AGP-pc and AGP/P25-pc, respectively. The irradiation is performed in a chloride-free water solution to exclude the possible chloride ion-driven transformation of Ag_3PO_4 to AgCl.

The XRD patterns for AGP-pc and AGP/P25-pc are shown in Fig. 1c and Fig. 1d, respectively. The photocorrosion leads to formation of metallic Ag adopting cubic close-packed crystal structure with space group $Fm\overline{3}m$ (ICDD 01-087-0579) in both AGP-pc and AGP/P25-pc. AGP-pc and AGP/P25-pc are further irradiated under VIS light in saline for 2 h (similar conditions as for their pristine counterparts). Clearly, a complete chloride ion-driven transformation of Ag_3PO_4 to AgCl is observed after 30 min irradiation for both AGP-pc and AGP/P25-pc. The transformation process differs for photocorroded materials compared to their pristine counterparts. This is explained by the fact that the structure of AGP-pc and AGP/P25-pc is already disturbed by the initial irradiation (the irradiation by which a pristine material is transformed into a photocorroded material). During VIS light irradiation, Ag^+ ions are transported to the surface of Ag_3PO_4 and vacancies in the structure are formed. Thus, the structure of Ag_3PO_4 is more likely to break down in the reaction with Cl^- ions present in saline. This results into a full transformation of Ag_3PO_4 to AgCl in photocorroded materials.

Representative SEM images of pristine, photocorroded and Ag_3PO_4 to AgCl transformed Ag_3PO_4 based materials are shown in Fig. 2. It is observed that the prepared pristine AGP (Fig. 2a) consists of nearly spherical particles with a relatively large diameter of ~0.5 μm. Regarding the pristine composite AGP/P25, the SEM (Fig. 2b) show significant morphological changes compared to the pristine AGP. In AGP/P25, the surface of the relatively large Ag_3PO_4 particles (~0.5 μm) is covered with smaller P25 TiO_2 nanoparticles. Thus, the morphology of AGP/P25 varies compared to that of AGP. Indeed, the average diameter of TiO_2 nanoparticles in the commercial P25 is ~25nm. This is clear from Fig. 2a and b. The original Ag_3PO_4 particles in AGP (Fig. 2a) are covered by TiO_2 nanoparticles in AGP/P25 (Fig. 2b). The photocorroded Ag_3PO_4 (AGP-pc) and its composite with TiO_2 (AGP/P25-pc) is shown on Fig. 2c and d, respectively. The surface of these materials is covered by smaller Ag particles with the crystallite size ranging from 100 nm to 2 μm for AGP-pc and from 30 nm to 100 nm for AGP/P25-pc. To distinguish the Ag in AGP and AGP/P25, Fig. 2d show a representative back-scattering electron imaging of AGP/P25-pc. The observed bright particles in Fig. 2d represents the distribution of Ag particles on the surface of AGP/P25-pc. On Fig. 2e and f, the shown SEM image is representative for AGP and AGP/P25 that underlined a partial-to-full Ag_3PO_4 to AgCl transformation. The significant change in morphology of t-AGP and t-AGP/P25 is attributed to the partial-to-full transformation of Ag_3PO_4 to AgCl. Clear AgCl particles are visible throughout the whole Ag_3PO_4 based materials. On Fig. 2e, the originally

274 ~0.5 μm large Ag_3PO_4 particles are covered by 50 - 150 nm large AgCl nanoparticles. Back-
275 scattering electron imaging of t-AGP/P25 is shown to indicate the presence of AgCl particles
276 (bright particles in Fig. 2f). The lower magnification if Fig. 2e and f is used on purpose
277 (compared to that in Fig. 2a-d) to show the partial-to-full Ag_3PO_4 to AgCl transformation on
278 the larger scale. To further confirm the presence of AgCl, representative EDS elemental
279 mapping (Fig. 3) is obtained from the BSE image (Fig. 3a) of t-AGP/P25 irradiated in saline
280 for 30 min. Clearly, as the Cl (Fig. 3b) and Ag (Fig. 3e) are distributed in the same area, the
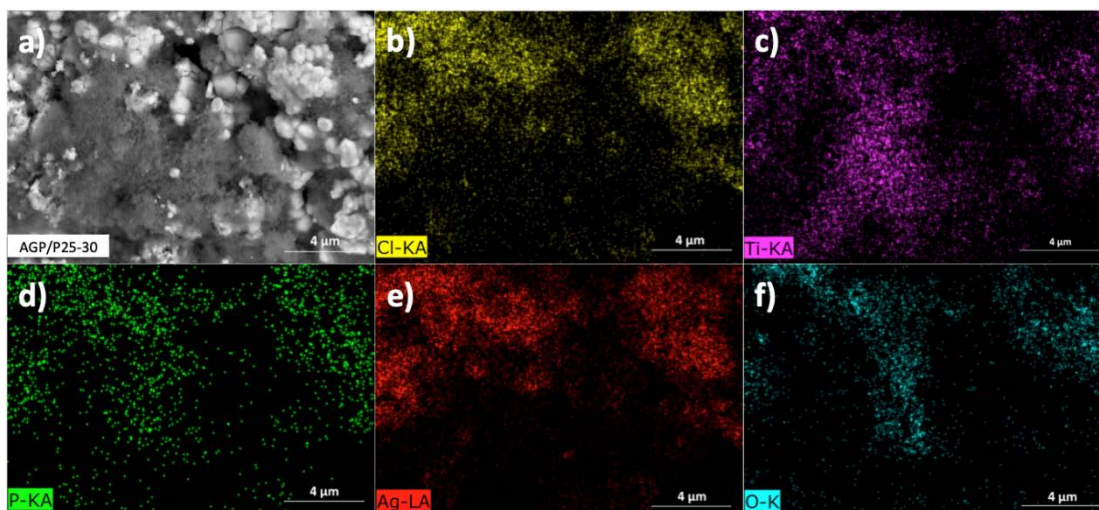281 presence of AgCl is confirmed.
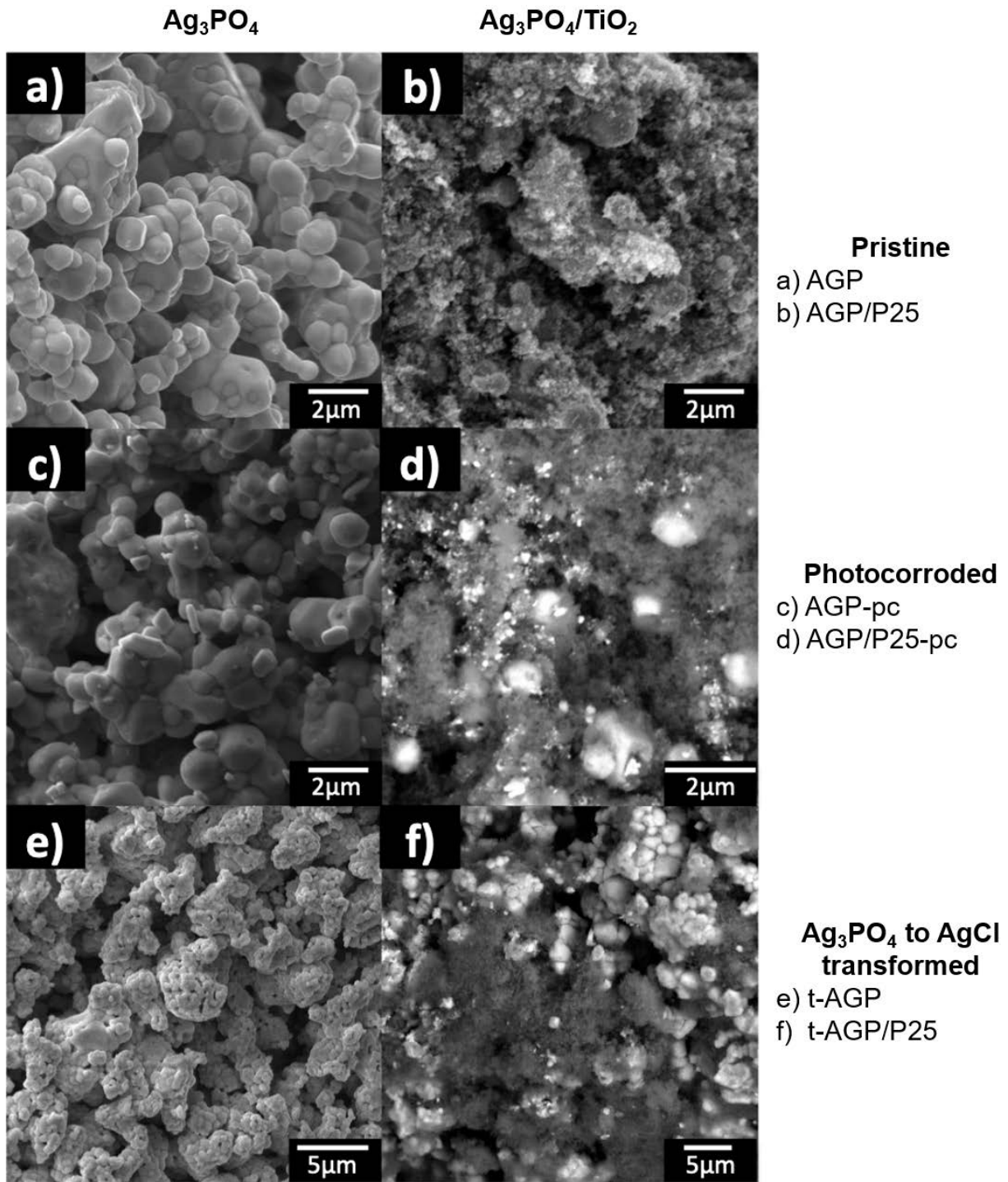
Fig. 2. SEM images of a) pristine Ag₃PO₄ (AGP); b) pristine Ag₃PO₄/TiO₂ composite (AGP/P25), their photocorroded counterparts c) AGP-pc; d) AGP/P25-pc, and Ag₃PO₄ to AgCl transformed counterparts e) t-AGP; f) t-AGP/P25

**Fig. 3.** a) BSE imaging of Ag₃PO₄ to AgCl transformed Ag₃PO₄/TiO₂ (t-AGP/P25) irradiated for 30 minutes under VIS light in saline and the corresponding elemental distribution of b) Cl, c) Ti, d) P, e) Ag and f) O.

Diffuse reflectance UV-VIS spectra (DRS) of AGP, AGP/P25, t-AGP and t-AGP/P25 is shown in Fig. 4a. For photocorroded AGP-pc and AGP-P25-pc, it was not possible to measure any reflectivity *due* to an extremely black color of the material (metallic Ag on the surface of Ag₃PO₄). This particular set is based on the presented XRD results (Fig. 1). As shown in Fig. 1, almost complete Ag₃PO₄ to AgCl transformation occurred in both AGP and AGP/P25. As a result, the initial AGP and AGP/P25 contains substantial amount of AgCl. Thus, for the purpose of comparison of the optical properties between pristine and partial-to-full Ag₃PO₄ to AgCl transformed materials, DRS of t-AGP and t-AGP/P25 is recorded. Thus, by such effort, the absorption properties of the pristine AGP and AGP/P25 (the initial material) is compared to the transformed t-AGP and t-AGP/P25 (the latter material after 2 h VIS light irradiation in saline), respectively. It can be clearly seen that the optical absorption cutoff wavelength is at ~475 nm for all Ag₃PO₄ based materials. Nevertheless, significant difference in reflectance is observed. The reflectance of AGP at 400 nm is ~10 %. All other Ag₃PO₄ based materials possess a stronger (~20 %) reflectance at 400 nm. Moreover, the reflectance of t-AGP and t-AGP/P25 is significantly lower in the wavelength range from 500 to 800 nm. The optical band gap is estimated from the corresponding Kubelka-Munk curves (Fig. 4b). Values of ~2.52 eV, ~2.48 eV, ~2.99 eV, and ~3.02 eV for AGP, AGP/P25, t-AGP, and t-AGP/P25 were determined, respectively. The difference in the reflectance and optical band gap energy is described as follows. Ag₃PO₄ have 90 % quantum efficiencies at ~420 nm. Thus, every detrimental aspect has a negative impact on its photoresponse in this specific wavelength. Here, TiO₂ in AGP/P25

312 and t-AGP/P25 lowers the absorption capacity of Ag_3PO_4. Moreover, the presence of AgCl on

313 the surface of t-AGP and t-AGP/P25 significantly changes the absorption capacities of Ag_3PO_4

314 and TiO_2. This is *due* to shading effect of AgCl (Slamet et al., 2005) and its discussed later in

315 the next chapter.
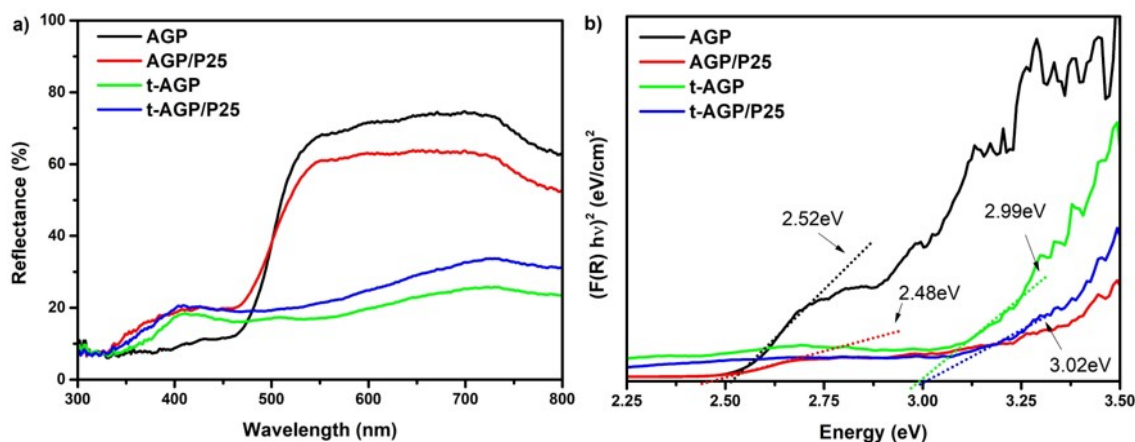
316

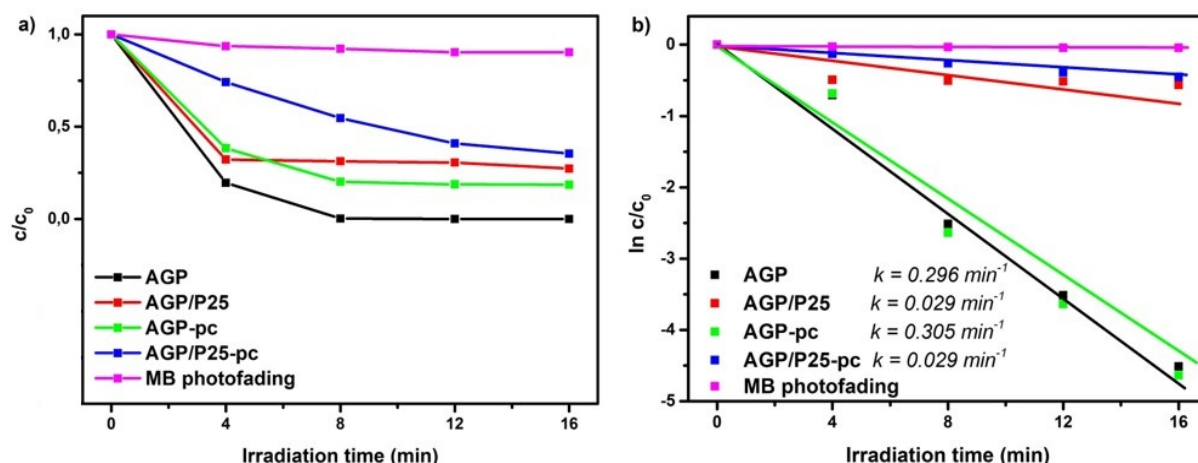317 **Fig. 4.** a) UV-VIS diffuse reflectance spectra and b) corresponding Kubelka-Munk curves of

318 Ag_3PO_4 (AGP) and Ag_3PO_4 /TiO_2 (AGP/P25) and their Ag_3PO_4 to AgCl transformed

319 counterparts (t-AGP and t-AGP/P25).

320

321 ***Photoinduced catalytic, antimicrobial, and antifungal performance of Ag₃PO₄ based***

322 ***materials***

323

324 The prepared pristine and photocorroded Ag_3PO_4 based materials are explored for the

325 photocatalytic degradation of MB under VIS light irradiation. Liquid phase photocatalytic

326 activity of a similar Ag_3PO_4 and Ag_3PO_4/TiO_2 material in chloride-free aqueous MB solution

327 is previously reported by our group (Baďurová et al., 2017). Herein, the structural changes and

328 their subsequent impact on photocatalytic activity of Ag_3PO_4 materials in saline is presented.

329 Thus, the MB powder was diluted in 0.80 % aqueous NaCl to obtain MB saline solution with

330 initial concentration of 10^{-5} M. Fig. 5 shows the liquid phase photocatalytic activity of all

331 Ag_3PO_4 based materials. The photodegradation of MB follows a pseudo-first-order reaction.

332 Thus its kinetics are expressed from the linear variation of ln c/c_0 as a function of time (Zlamal

333 et al., 2007). The resulting kinetic rate constants are given in Fig. 5.

Fig. 5. Liquid phase photocatalysis: degradation rates of methylene blue (MB) for pristine Ag$_3$PO$_4$ (AGP) and Ag$_3$PO$_4$ /TiO$_2$ (AGP/P25), their photocorroded counterparts AGP-pc and AGP/P25-pc, and the corresponding rate constants *k*.

Results show that AGP and AGP-pc possess enhanced photocatalytic activity compared to their TiO$_2$-composite counterparts. A full photodegradation of MB is achieved after 16 min using AGP and ~90 % using AGP-pc. More than 50 % of MB is photodegraded using AGP/P25 and AGP/P25-pc. The potential reasons for the enhanced photocatalytic activity of AGP and AGP-pc compared to their TiO$_2$-composite counterparts are following: 1) VIS light irradiation is used for MB photodegradation. Therefore, composites with TiO$_2$ possess decreased photocatalytic activities *due* to the inefficient absorption of the incident VIS light by TiO$_2$. As seen on SEM (Fig. 2b) TiO$_2$ shades Ag$_3$PO$_4$; 2) the type-II heterojunction Ag$_3$PO$_4$/TiO$_2$ is not efficient. We believe this is *due* to the chloride-present environment used during photocatalysis. As discussed in the characterization part (XRD and SEM, Fig. 1-3), a partial-to-full transformation of Ag$_3$PO$_4$ to AgCl occurred under these specific conditions. This means that the efficient charge carrier separation between TiO$_2$ and Ag$_3$PO$_4$ is negligible. The possibility that the synthesis of Ag$_3$PO$_4$/TiO$_2$ composite is inefficient is excluded. Our previous report (Baďurová et al., 2017) show the enhanced photocatalytic performance of AGP/P25 in a chloride-free environment. Moreover, the Ag$_3$PO$_4$ to AgCl transformation has to be considered. Although the incident VIS light absorption by AgCl is limited, there are numerous reports which show its photocatalytic activity *due* to the effective e$^-$ transfer from the photoexcited AgCl and plasmon-excited metallic Ag particles to Ag$_3$PO$_4$ (Guo et al., 2018; Luo et al., 2013; Shi et al., 2013; Zhao et al., 2018). Obviously, such e$^-$ transfer mechanism is only possible in materials where the full Ag$_3$PO$_4$ to AgCl transformation did not occur. Moreover, the presence of chloride ions in the photocatalytic system (stemming from saline) is responsible for the

generation of chloride-based reactive species such as chlorine radicals and dichlorine radicals (Huang et al., 2018; Kiwi et al., 2000; Yang et al., 2014). Such chloride-based radicals are efficient in the degradation of pollutants (Huang et al., 2018; Kiwi et al., 2000; Yang et al., 2014).

At last, *S. maltophilia* and *C. albicans* is chosen as a model bacteria and fungi for further photoinduced antimicrobial and antifungal inactivation tests. *S. maltophilia* is an aerobic, non-fermentative, gram-negative, multi-drug-resistant pathogen found in aquatic environments (Alavi et al., 2014; Brooke et al., 2012). *S. maltophilia* frequently colonizes fluids used in hospitals (e.g., irrigation solutions, intravenous fluids, etc.) and is found in patient secretions (e.g., urine, exudates, etc.) causing both mild and severe life-threating infectious complications in immunocompromised individuals. *C. albicans* is an ubiquitous polymorphic specie and the most common opportunistic pathogen (Haghighi eet al., 2012; Moyes et al., 2015). *C. albicans* is found mainly in people with impaired immune system (e.g., cancer, transplant, HIV patients, etc.). Their photocatalytic inactivation using Ag_3PO_4 materials under VIS light is shown in Fig. 6. Both *S. maltophilia* and *C. albicans* are susceptible to the VIS photoinduced inactivation on all Ag_3PO_4 based materials. The applied irradiation did not induce the inactivation of the microorganisms on control materials.
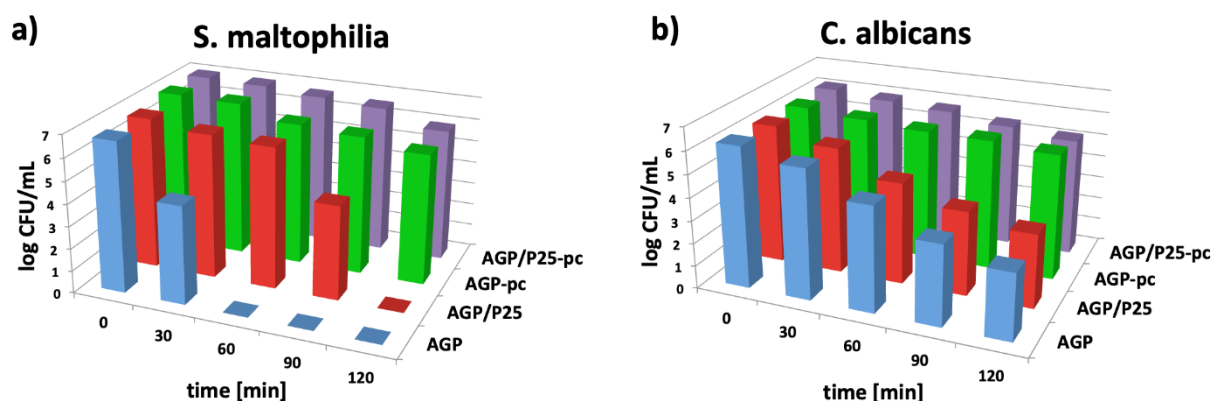
Fig. 6. Photoinduced antimicrobial and antifungal inactivation of a) *S. maltophilia* and b) *C. Albicans* on Ag_3PO_4 based materials.

As seen in Fig. 6a, the cell survival of *S. maltophilia* bacterial strains is reduced by 100 % after 60 min and 120 min using AGP and AGP/P25, respectively. The more efficient antimicrobial performance of AGP is ascribed to a higher content of Ag_3PO_4 in AGP compared to that in AGP/P25. Indeed, Ag_3PO_4 is an effective VIS light-driven photocatalyst in contrast to TiO_2, which is mainly photoactive in UV region. The fungi of *C. albicans* are more resistant

387 compared to the bacterial strains (Fig. 6b). The photoinduced inactivation is reduced to 50 %
388 for both AGP and AGP/P25 (Fig. 6b). This significant decrease in the photoinduced inactivation
389 is caused by differences in the cell wall structures between *S. maltophilia* and *C. albicans*. In
390 general, a gram-negative bacteria possess a double lipid bilayer (an inner and an outer
391 membrane) separated by periplasmatic space and peptidoglycan (Regmi et al., 2018; Rodrigues-
392 Silva et al., 2017, 2017; Wolfrum et al., 2002). The outer membrane contains porins and
393 lipoproteins and is decorated with lipopolysaccharide chains with a negative charge. Fungi, on
394 the other hand, have an outer cell wall composed of polysaccharides such as mannan, β-glucan
395 and chitin and these cells do not have a pronounced negative charge (Regmi et al., 2018;
396 Rodrigues-Silva et al., 2017, 2017; Wolfrum et al., 2002). Therefore, to kill a fungal cell, the
397 required concentrations of ROS is significantly higher compared to the concentration of ROS
398 needed to kill a bacterial cell.

399   Photoinduced inactivation tests using similar pathogens are also studied on
400 photocorroded AGP-pc and AGP/P25-pc. In general, the photoinduced inactivation
401 performance is significantly lower compared to that of pristine AGP and AGP/P25. The reason
402 for this is two-fold: i) the presence of metallic Ag on the surface of AGP-pc and AGP/P25-pc
403 decrease the photoinduced inactivation activity of Ag_3PO_4 and TiO_2 *due* to a shading effect
404 (Slamet et al., 2005). This means that the metallic Ag blocks the incident light absorption by
405 Ag_3PO_4 and TiO_2 and reduces their photoexcitation capacity, and ii) after photocorrosion, the
406 released Ag^+ ions on the surface are available for immediate reaction with Cl^- ions in saline.
407 Thus Ag^+ ions accelerates the transformation of Ag_3PO_4 to AgCl. As already discussed, and
408 shown (Fig. 1), a complete transformation of Ag_3PO_4 to AgCl occurs during the procedure to
409 obtain photocorroded AGP-pc and AGP/P25-pc. Therefore, in the case of AGP-pc and
410 AGP/P25-pc the photoinduced inactivation ability of Ag_3PO_4 and Ag_3PO_4/TiO_2 is rather the
411 photoinduced inactivation ability of AgCl and $AgCl/TiO_2$, respectively.

412 Additional aspects need to be considered regarding the antibacterial and antifungal performance
413 of all Ag_3PO_4 based materials. AgCl is prone to disintegration (to Ag^+ and Cl^-) under VIS light
414 irradiation. As reported (Kim et al., 2016), the newly formed Ag^+ ions induce the production of
415 ROS by disrupting metabolic pathway and increase membrane permeability, which leads to
416 bacterial cell death. Moreover, photogenerated chloride-based reactive species (e.g., chlorine
417 and dichlorine radicals) disrupt the cell membrane (Dröge et al., 2002; Nishikiori et al., 2008;
418 Watts et al., 2007). This leads to cell death. Although AgCl is known for its photoinduced
419 inactivation ability, Ag_3PO_4 is a superior photocatalyst with a more efficient charge transfer
420 and lower e^-/h^+ recombination rate. At last, the concentration of Ag^+ in Ag_3PO_4 based materials

421 can influence their antibacterial and antifungal performance. Ag^+ kills bacteria by hindering the

422 DNA replication and inhibits the expression of ribosomal proteins/enzymes for ATP hydrolysis

423 (Lee et al., 2005; Liu et al., 2012; Markowska et al., 2013). The VIS light- and chloride-ion

424 driven transformation primarily transforms Ag_3PO_4 to AgCl. However, inconsiderable amount

425 of Ag^+ is also generated from Ag_3PO_4. The concentration of Ag^+ in Ag_3PO_4 based materials in

426 saline under VIS light irradiation (during 2.5 h irradiation) is previously reported (Hong et al.,

427 2016). After 30 min of VIS light irradiation in a chloride-present environment, the

428 concentration of Ag^+ increased from 0 to ~2.5 ppm and reaches plateau (Hong et al., 2016). A

429 comparable amount of Ag^+ is generated in dark (Hong et al., 2016). This suggest that Ag^+ can

430 be generated in a chloride-present environment without any irradiation. Indeed, the Ag_3PO_4

431 partially ionizes in aqueous solutions to release Ag^+ ions with stable and controlled rate (Lee et

432 al., 2005; Liu et al., 2012; Markowska et al., 2013). Nevertheless, the concentration of the

433 generated Ag^+ (both under the VIS irradiation and in the dark) is similar in Ag_3PO_4 based

434 materials. This suggest that the amount of generated Ag^+ is dependent on the exposed area of

435 Ag_3PO_4 to the saline and/or to the incident VIS light. Therefore, although the concentration of

436 Ag^+ is not quantified in the present work, it is assumed that the generation-ability of our studied

437 Ag_3PO_4 based materials to generate Ag^+ follows the order AGP > AGP/P25 > AGP-pc >

438 AGP/P25-pc (where AGP generates the most Ag^+). The reasoning is following. Pristine AGP

439 contains only Ag_3PO_4 therefore the material is fully exposed to the saline and the incident VIS

440 light. Thus, generates the most Ag^+. Lower amount of Ag_3PO_4 is exposed to its surroundings in

441 pristine AGP/P25 *due* to TiO_2 which shades Ag_3PO_4. In the case of AGP-pc, the surface is

442 covered by metallic Ag which shades Ag_3PO_4. At last, in the case of AGP/P25-pc, the surface

443 covered by TiO_2 and metallic Ag shades Ag_3PO_4.

444   When considering all previous reports and results shown herein, it is obvious that the

445 photocatalytic activity of pristine Ag_3PO_4 and its composite with TiO_2 is significantly enhanced

446 compared to their photocorroded counterparts. Nevertheless, the partial-to-full transformation

447 of Ag_3PO_4 to AgCl and/or Ag is detrimental and have a negative effect on the structural and

448 morphological properties and influences the photocatalytic, antibacterial, and antifungal

449 performance of the material.

450

451   **Conclusions**

452

453 In conclusion, efficient synthesis of cubic Ag_3PO_4 and its composite with TiO_2 is demonstrated

454 in this work. Presented VIS light-driven and chloride ion-drive partial-to-full transformation of

Ag$_3$PO$_4$ to AgCl and/or Ag shows a significant impact on the crystal structure and on the morphology of Ag$_3$PO$_4$ and its composite with TiO$_2$. The photocorroded AGP-pc and AGP/P25-pc possess decreased photoinduced catalytic, antibacterial, and antifungal performance compared to their pristine counterparts (AGP and AGP/P25). The released metallic Ag in AGP-pc and AGP/P25-pc accelerates the transformation of Ag$_3$PO$_4$ to AgCl thus negatively affecting its photocatalytic properties. The pristine AGP and AGP/P25 possess enhanced photocatalytic activities compared to their photocorroded counterparts in saline. Nevertheless, a chloride ion-driven and VIS light-driven partial-to-full transformation of Ag$_3$PO$_4$ to AgCl also occurs during the photoinduced catalytic, antimicrobial, and antifungal tests. Results shown herein points to the fact that photocatalytic properties of Ag$_3$PO$_4$ in chloride ions containing environments are often presented inappropriately and the actual contribution of Ag$_3$PO$_4$ in photocatalytic processes is much lower than presented.

Conflict of interest

On behalf of all authors, the corresponding author states that there is no conflict of interest.

References

Alavi, P., Starcher, M. R., Thallinger, G. G., Zachow, C., Müller, H., & Berg, G. (2014). Stenotrophomonas comparative genomics reveals genes and functions that differentiate beneficial and pathogenic bacteria. *BMC Genomics*, *15*(1), 482. https://doi.org/10.1186/1471-2164-15-482

Baďurová, K., Monfort, O., Satrapinskyy, L., Dworniczek, E., Gościniak, G., & Plesch, G. (2017). Photocatalytic activity of Ag3PO4 and some of its composites under non-filtered and UV-filtered solar-like radiation. *Ceramics International*, *43*(4), 3706–3712. https://doi.org/10.1016/j.ceramint.2016.11.217

Beketova, D., Motola, M., Sopha, H., Michalicka, J., Cicmancova, V., Dvorak, F., … Macak, J. M. (2020). One-step decoration of TiO2 nanotubes with Fe3O4 nanoparticles: synthesis, and photocatalytic, and magnetic properties. *ACS Applied Nano Materials*,

acsanm.9b02337. https://doi.org/10.1021/acsanm.9b02337

Bi, Y., Hu, H., Ouyang, S., Lu, G., Cao, J., & Ye, J. (2012). Photocatalytic and photoelectric properties of cubic Ag3PO4 sub-microcrystals with sharp corners and edges. *Chemical Communications*, *48*(31), 3748–3750. https://doi.org/10.1039/c2cc30363a

Bi, Y., Ouyang, S., Cao, J., & Ye, J. (2011). Facile synthesis of rhombic dodecahedral AgX/Ag3PO4 (X = Cl, Br, I) heterocrystals with enhanced photocatalytic properties and stabilities. *Physical Chemistry Chemical Physics*, *13*(21), 10071–10075. https://doi.org/10.1039/c1cp20488b

Brooke, J. S. (2012, January). Stenotrophomonas maltophilia: An emerging global opportunistic pathogen. *Clinical Microbiology Reviews*. https://doi.org/10.1128/CMR.00019-11

Chatterjee, D., & Dasgupta, S. (2005, October). Visible light induced photocatalytic degradation of organic pollutants. *Journal of Photochemistry and Photobiology C: Photochemistry Reviews*. https://doi.org/10.1016/j.jphotochemrev.2005.09.001

Chen, X., Hu, B., Xing, X., Liu, Z., Zuo, Y., & Xiang, Q. (2015). Preparation of grafted cationic polymer/silver chloride modified cellulose fibers and their antibacterial properties. *Journal of Applied Polymer Science*, *132*(25). https://doi.org/10.1002/APP.42092

Dong, L., Liang, D., & Gong, R. (2012). In Situ Photoactivated AgCl/Ag Nanocomposites with Enhanced Visible Light Photocatalytic and Antibacterial Activity. *European Journal of Inorganic Chemistry*, *2012*(19), 3200–3208. https://doi.org/10.1002/ejic.201200172

Dröge, W. (2002). Free radicals in the physiological control of cell function. *Physiological Reviews*. American Physiological Society. https://doi.org/10.1152/physrev.00018.2001

Du, J., & Gebicki, J. M. (2004). Proteins are major initial cell targets of hydroxyl free radicals. *International Journal of Biochemistry and Cell Biology*, *36*(11), 2334–2343. https://doi.org/10.1016/j.biocel.2004.05.012

F. Haghighi. S.R. Mohammadi, P. Mohammadi, M. Eskandaru, S. H. (2012). The evaluation of Candida albicans biofilms formation on silicone catheter, PVC and glass coated with titanium dioxide nanoparticles by XTT method and ATPase assay. | Sigma-Aldrich. Retrieved January 20, 2020, from https://www.sigmaaldrich.com/catalog/papers/23173628

Guo, J., Shi, H., Huang, X., Shi, H., & An, Z. (2018). AgCl/Ag3PO4: A stable Ag-Based nanocomposite photocatalyst with enhanced photocatalytic activity for the degradation of parabens. *Journal of Colloid and Interface Science*, *515*, 10–17. https://doi.org/10.1016/j.jcis.2018.01.015

Hewer, T. L. R., Machado, B. C., Freire, R. S., & Guardani, R. (2014). Ag3PO4 sunlight-induced photocatalyst for degradation of phenol. *RSC Advances*, *4*(65), 34674–34680. https://doi.org/10.1039/c4ra04457f

Hoffmann, M. R., Martin, S. T., Choi, W., & Bahnemannt, D. W. (1995). *Environmental Applications of Semiconductor Photocatalysis*. *Chem. Rev* (Vol. 95).

Hong, X., Li, M., Shan, S., Hui, K. S., Mo, M., & Yuan, X. (2016). Chloride ion-driven transformation from Ag3PO4 to AgCl on the hydroxyapatite support and its dual antibacterial effect against Escherichia coli under visible light irradiation. *Environmental Science and Pollution Research*, *23*(13), 13458–13466. https://doi.org/10.1007/s11356-016-6530-7

Houas, A., Lachheb, H., Ksibi, M., Elaloui, E., Guillard, C., & Herrmann, J. M. (2001). Photocatalytic degradation pathway of methylene blue in water. *Applied Catalysis B: Environmental*, *31*(2), 145–157. https://doi.org/10.1016/S0926-3373(00)00276-9

Hu, C., Lan, Y., Qu, J., Hu, X., & Wang, A. (2006). Ag/AgBr/TiO2 visible light photocatalyst for destruction of azodyes and bacteria. *Journal of Physical Chemistry B*, *110*(9), 4066–4072. https://doi.org/10.1021/jp0564400

Huang, W., Bianco, A., Brigante, M., & Mailhot, G. (2018). UVA-UVB activation of hydrogen peroxide and persulfate for advanced oxidation processes: Efficiency, mechanism and effect of various water constituents. *Journal of Hazardous Materials*, *347*, 279–287. https://doi.org/10.1016/j.jhazmat.2018.01.006

Kang, Y., Jung, J.-Y., Cho, D., Kwon, O., Cheon, J., & Park, W. (2016). Antimicrobial Silver Chloride Nanoparticles Stabilized with Chitosan Oligomer for the Healing of Burns. *Materials*, *9*(4), 215. https://doi.org/10.3390/ma9040215

Kim, M. K., Yeo, B. E., Park, H., Huh, Y. D., Kwon, C., & Yun, H. S. (2016). Dual effect of the Cubic Ag3PO4 crystal on Pseudomonas syringae growth and plant immunity. *Plant Pathology Journal*, *32*(2), 168–170. https://doi.org/10.5423/PPJ.NT.09.2015.0191

Kiwi, J., Lopez, A., & Nadtochenko, V. (2000). Mechanism and kinetics of the OH-radical intervention during Fenton oxidation in the presence of a significant amount of radical scavenger (Cl-). *Environmental Science and Technology*, *34*(11), 2162–2168. https://doi.org/10.1021/es991406i

Krbal, M., Ng, S., Motola, M., Hromadko, L., Dvorak, F., Prokop, V., … Macak, J. M. (2019). Sulfur treated 1D anodic TiO2 nanotube layers for significant photo- and electroactivity enhancement. *Applied Materials Today*, *17*, 104–111. https://doi.org/10.1016/j.apmt.2019.07.018

Kumar, S., Surendar, T., & Shanker, V. (2014). Template-free and eco-friendly synthesis of hierarchical Ag 3PO4 microcrystals with sharp corners and edges for enhanced photocatalytic activity under visible light. *Materials Letters*, *123*, 172–175. https://doi.org/10.1016/j.matlet.2014.02.106

Lapworth, D. J., Baran, N., Stuart, M. E., & Ward, R. S. (2012, April). Emerging organic contaminants in groundwater: A review of sources, fate and occurrence. *Environmental Pollution*. https://doi.org/10.1016/j.envpol.2011.12.034

Lee, D., Cohen, R. E., & Rubner, M. F. (2005). Antibacterial properties of Ag nanoparticle loaded multilayers and formation of magnetically directed antibacterial microparticles. *Langmuir*, *21*(21), 9651–9659. https://doi.org/10.1021/la0513306

Liang, Q., Shi, Y., Ma, W., Li, Z., & Yang, X. (2012). Enhanced photocatalytic activity and structural stability by hybridizing Ag3PO4 nanospheres with graphene oxide sheets. *Physical Chemistry Chemical Physics*, *14*(45), 15657–15665. https://doi.org/10.1039/c2cp42465g

Liu, B., Xue, Y., Zhang, J., Han, B., Zhang, J., Suo, X., … Shi, H. (2017). Visible-light-driven TiO2/Ag3PO4 heterostructures with enhanced antifungal activity against agricultural pathogenic fungi Fusarium graminearum and mechanism insight. *Environmental Science: Nano*, *4*(1), 255–264. https://doi.org/10.1039/c6en00415f

Liu, J. K., Luo, C. X., Wang, J. D., Yang, X. H., & Zhong, X. H. (2012). Controlled synthesis of silver phosphate crystals with high photocatalytic activity and bacteriostatic activity. *CrystEngComm*, *14*(24), 8714–8721. https://doi.org/10.1039/c2ce25604e

Luo, G., Jiang, X., Li, M., Shen, Q., Zhang, L., & Yu, H. (2013). Facile fabrication and enhanced photocatalytic performance of Ag/AgCl/rGO heterostructure photocatalyst. *ACS Applied Materials and Interfaces*, *5*(6), 2161–2168. https://doi.org/10.1021/am303225n

Malato, S., Fernández-Ibáñez, P., Maldonado, M. I., Blanco, J., & Gernjak, W. (2009, September 15). Decontamination and disinfection of water by solar photocatalysis: Recent overview and trends. *Catalysis Today*. https://doi.org/10.1016/j.cattod.2009.06.018

Markowska, K., Grudniak, A. M., & Wolska, K. I. (2013). Silver nanoparticles as an alternative strategy against bacterial biofilms. *Acta Biochimica Polonica*. https://doi.org/10.18388/abp.2013_2016

Michal, R., Dworniczek, E., Čaplovičová, M., Gregor, M., Čaplovič, L., Seniuk, A., … Plesch, G. (2014). Photocatalytic and photodisinfectant activity of sulfated and Eu doped anatase

against clinically important microorganisms. *Ceramics International*, *40*(4), 5745–5756. https://doi.org/10.1016/j.ceramint.2013.11.013

Monfort, O., & Plesch, G. (2018, July 1). Bismuth vanadate-based semiconductor photocatalysts: a short critical review on the efficiency and the mechanism of photodegradation of organic pollutants. *Environmental Science and Pollution Research*. Springer Verlag. https://doi.org/10.1007/s11356-018-2437-9

Motola, M., Baudys, M., Zazpe, R., Krbal, M., Michalička, J., Rodriguez-Pereira, J., … Macak, J. M. (2019). 2D MoS $_2$ nanosheets on 1D anodic TiO $_2$ nanotube layers: an efficient co-catalyst for liquid and gas phase photocatalysis. *Nanoscale*, *11*(48), 23126–23131. https://doi.org/10.1039/C9NR08753B

Motola, M., Dworniczek, E., Satrapinskyy, L., Chodaczek, G., Grzesiak, J., Gregor, M., … Plesch, G. (2019). UV light-induced photocatalytic, antimicrobial, and antibiofilm performance of anodic TiO $_2$ nanotube layers prepared on titanium mesh and Ti sputtered on silicon. *Chemical Papers*, *73*(5), 1163–1172. https://doi.org/10.1007/s11696-018-0667-4

Motola, M., Satrapinskyy, L., Čaplovicová, M., Roch, T., Gregor, M., Grančič, B., … Plesch, G. (2018). Enhanced photocatalytic activity of hydrogenated and vanadium doped TiO $_2$ nanotube arrays grown by anodization of sputtered Ti layers. *Applied Surface Science*, *434*, 1257–1265. https://doi.org/10.1016/j.apsusc.2017.11.253

Motola, M., Satrapinskyy, L., Roch, T., Šubrt, J., Kupčík, J., Klementová, M., … Plesch, G. (2017). Anatase TiO2nanotube arrays and titania films on titanium mesh for photocatalytic NOXremoval and water cleaning. *Catalysis Today*, *287*, 59–64. https://doi.org/10.1016/j.cattod.2016.10.011

Moyes, D. L., Richardson, J. P., & Naglik, J. R. (2015). *Candida albicans*- epithelial interactions and pathogenicity mechanisms: scratching the surface. *Virulence*, *6*(4), 338–346. https://doi.org/10.1080/21505594.2015.1012981

Nishikiori, R., Nomura, Y., Sawajiri, M., Masuki, K., Hirata, I., & Okazaki, M. (2008). Influence of chlorine dioxide on cell death and cell cycle of human gingival fibroblasts. *Journal of Dentistry*, *36*(12), 993–998. https://doi.org/10.1016/j.jdent.2008.08.006

Overmyer, K., Brosché, M., & Kangasjärvi, J. (2003, July 1). Reactive oxygen species and hormonal control of cell death. *Trends in Plant Science*. Elsevier Ltd. https://doi.org/10.1016/S1360-1385(03)00135-3

Piccirillo, C., Pinto, R. A., Tobaldi, D. M., Pullar, R. C., Labrincha, J. A., Pintado, M. M. E., & Castro, P. M. L. (2015). Light induced antibacterial activity and photocatalytic properties of Ag/3PO4 -based material of marine origin. *Journal of Photochemistry and Photobiology A: Chemistry*, *296*, 40–47. https://doi.org/10.1016/j.jphotochem.2014.09.012

Regmi, C., Joshi, B., Ray, S. K., Gyawali, G., & Pandey, R. P. (2018). Understanding Mechanism of Photocatalytic Microbial Decontamination of Environmental Wastewater. *Frontiers in Chemistry*, *6*. https://doi.org/10.3389/fchem.2018.00033

Rehan, M., Khattab, T. A., Barohum, A., Gätjen, L., & Wilken, R. (2018). Development of Ag/AgX (X = Cl, I) nanoparticles toward antimicrobial, UV-protected and self-cleanable viscose fibers. *Carbohydrate Polymers*, *197*, 227–236. https://doi.org/10.1016/j.carbpol.2018.06.010

Rodrigues-Silva, C., Miranda, S. M., Lopes, F. V. S., Silva, M., Dezotti, M., Silva, A. M. T., … Pinto, E. (2017). Bacteria and fungi inactivation by photocatalysis under UVA irradiation: liquid and gas phase. *Environmental Science and Pollution Research*, *24*(7), 6372–6381. https://doi.org/10.1007/s11356-016-7137-8

Roy, M., Fielding, G. A., Beyenal, H., Bandyopadhyay, A., & Bose, S. (2012). Mechanical, in vitro antimicrobial, and biological properties of plasma-sprayed silver-doped

hydroxyapatite coating. *ACS Applied Materials and Interfaces*, *4*(3), 1341–1349. https://doi.org/10.1021/am201610q

Sadowski, R., Strus, M., Buchalska, M., Heczko, P. B., & Macyk, W. (2015). Visible light induced photocatalytic inactivation of bacteria by modified titanium dioxide films on organic polymers. *Photochemical and Photobiological Sciences*, *14*(3), 514–519. https://doi.org/10.1039/c4pp00270a

Schneider, J., Matsuoka, M., Takeuchi, M., Zhang, J., Horiuchi, Y., Anpo, M., & Bahnemann, D. W. (2014, October 8). Understanding TiO2photocatalysis: Mechanisms and materials. *Chemical Reviews*. American Chemical Society. https://doi.org/10.1021/cr5001892

Schwarzenbach, R. P., Escher, B. I., Fenner, K., Hofstetter, T. B., Johnson, C. A., Von Gunten, U., & Wehrli, B. (2006, August 25). The challenge of micropollutants in aquatic systems. *Science*. https://doi.org/10.1126/science.1127291

Serpone, N., Maruthamuthu, P., Pichat, P., Pelizzetti, E., & Hidaka, H. (1995). Exploiting the interparticle electron transfer process in the photocatalysed oxidation of phenol, 2-chlorophenol and pentachlorophenol: chemical evidence for electron and hole transfer between coupled semiconductors. *Journal of Photochemistry and Photobiology, A: Chemistry*, *85*(3), 247–255. https://doi.org/10.1016/1010-6030(94)03906-B

Shi, H., Chen, J., Li, G., Nie, X., Zhao, H., Wong, P. K., & An, T. (2013). Synthesis and characterization of novel plasmonic Ag/AgX-CNTs (X = Cl, Br, I) nanocomposite photocatalysts and synergetic degradation of organic pollutant under visible light. *ACS Applied Materials and Interfaces*, *5*(15), 6959–6967. https://doi.org/10.1021/am401459c

Silvestry-Rodriguez, N., Sicairos-Ruelas, E. E., Gerba, C. P., & Bright, K. R. (2007). Silver as a disinfectant. *Reviews of Environmental Contamination and Toxicology*, *191*, 23–45. https://doi.org/10.1007/978-0-387-69163-3_2

Slamet, Nasution, H. W., Purnama, E., Kosela, S., & Gunlazuardi, J. (2005). Photocatalytic reduction of CO2 on copper-doped Titania catalysts prepared by improved-impregnation method. *Catalysis Communications*, *6*(5), 313–319. https://doi.org/10.1016/j.catcom.2005.01.011

Sopha, H., Hromadko, L., Motola, M., & Macak, J. M. (2020). Fabrication of TiO2 nanotubes on Ti spheres using bipolar electrochemistry. *Electrochemistry Communications*, *111*, 106669. https://doi.org/10.1016/j.elecom.2020.106669

Teng, W., Li, X., Zhao, Q., Zhao, J., & Zhang, D. (2012). In situ capture of active species and oxidation mechanism of RhB and MB dyes over sunlight-driven Ag/Ag 3PO 4 plasmonic nanocatalyst. *Applied Catalysis B: Environmental*, *125*, 538–545. https://doi.org/10.1016/j.apcatb.2012.05.043

Wang, B., Gu, X., Zhao, Y., & Qiang, Y. (2013). A comparable study on the photocatalytic activities of Ag 3 PO 4 , AgBr and AgBr/Ag 3 PO 4 hybrid microstructures. *Applied Surface Science*, *283*, 396–401. https://doi.org/10.1016/j.apsusc.2013.06.121

Watts, M. J., & Linden, K. G. (2007). Chlorine photolysis and subsequent OH radical production during UV treatment of chlorinated water. *Water Research*, *41*(13), 2871–2878. https://doi.org/10.1016/j.watres.2007.03.032

Wetchakun, K., Wetchakun, N., & Sakulsermsuk, S. (2019, March 25). An overview of solar/visible light-driven heterogeneous photocatalysis for water purification: TiO2- and ZnO-based photocatalysts used in suspension photoreactors. *Journal of Industrial and Engineering Chemistry*. Korean Society of Industrial Engineering Chemistry. https://doi.org/10.1016/j.jiec.2018.11.025

Wolfrum, E. J., Huang, J., Blake, D. M., Maness, P. C., Huang, Z., Fiest, J., & Jacoby, W. A. (2002). Photocatalytic oxidation of bacteria, bacterial and fungal spores, and model biofilm components to carbon dioxide on titanium dioxide-coated surfaces. *Environmental Science and Technology*, *36*(15), 3412–3419. https://doi.org/10.1021/es011423j

Wu, L., Xie, Q., Lv, Y., Zhang, Z., Wu, Z., Liang, X., … Nie, Y. (2019). Degradation of methylene blue by dielectric barrier discharge plasma coupled with activated carbon supported on polyurethane foam. *RSC Advances*, *9*(45), 25967–25975. https://doi.org/10.1039/c9ra05238k

Yang, X., Qin, J., Jiang, Y., Chen, K., Yan, X., Zhang, D., … Tang, H. (2015). Fabrication of P25/Ag3PO4/graphene oxide heterostructures for enhanced solar photocatalytic degradation of organic pollutants and bacteria. *Applied Catalysis B: Environmental*, *166–167*, 231–240. https://doi.org/10.1016/j.apcatb.2014.11.028

Yang, Y., Pignatello, J. J., Ma, J., & Mitch, W. A. (2014). Comparison of halide impacts on the efficiency of contaminant degradation by sulfate and hydroxyl radical-based advanced oxidation processes (AOPs). *Environmental Science and Technology*, *48*(4), 2344–2351. https://doi.org/10.1021/es404118q

Yao, W., Zhang, B., Huang, C., Ma, C., Song, X., & Xu, Q. (2012). Synthesis and characterization of high efficiency and stable Ag 3PO 4/TiO 2 visible light photocatalyst for the degradation of methylene blue and rhodamine B solutions. *Journal of Materials Chemistry*, *22*(9), 4050–4055. https://doi.org/10.1039/c2jm14410g

Yi, Z., Ye, J., Kikugawa, N., Kako, T., Ouyang, S., Stuart-Williams, H., … Withers, R. L. (2010). An orthophosphate semiconductor with photooxidation properties under visible-light irradiation. *Nature Materials*, *9*(7), 559–564. https://doi.org/10.1038/nmat2780

Zhang, H., Huang, H., Ming, H., Li, H., Zhang, L., Liu, Y., & Kang, Z. (2012). Carbon quantum dots/Ag 3PO 4 complex photocatalysts with enhanced photocatalytic activity and stability under visible light. *Journal of Materials Chemistry*, *22*(21), 10501–10506. https://doi.org/10.1039/c2jm30703k

Zhang, L., Zhang, H., Huang, H., Liu, Y., & Kang, Z. (2012). Ag3PO4/SnO2 semiconductor nanocomposites with enhanced photocatalytic activity and stability. *New Journal of Chemistry*, *36*(8), 1541–1544. https://doi.org/10.1039/c2nj40206h

Zhang, S., Gu, X., Zhao, Y., & Qiang, Y. (2015). Effect of annealing temperature and time on structure, morphology and visible-light photocatalytic activities Ag$_3$PO$_4$ microparticles. *Materials Science and Engineering B: Solid-State Materials for Advanced Technology*, *201*, 57–65. https://doi.org/10.1016/j.mseb.2015.08.005

Zhao, F. M., Pan, L., Wang, S., Deng, Q., Zou, J. J., Wang, L., & Zhang, X. (2014). Ag 3 PO 4 /TiO 2 composite for efficient photodegradation of organic pollutants under visible light. *Applied Surface Science*, *317*, 833–838. https://doi.org/10.1016/j.apsusc.2014.09.022

Zhao, W., Ma, W., Chen, C., Zhao, J., & Shuai, Z. (2004). Efficient Degradation of Toxic Organic Pollutants with Ni2O 3/TiO2-xBx under Visible Irradiation. *Journal of the American Chemical Society*, *126*(15), 4782–4783. https://doi.org/10.1021/ja0396753

Zhao, X., Song, L., & Zhang, S. (2018). Synthesis of AgCl/Ag 3 PO 4 Composite Photocatalysts and Study on Photodegradation Activity Based on a Continuous Reactor. *Photochemistry and Photobiology*, *94*(3), 484–490. https://doi.org/10.1111/php.12875

Zlamal, M., Macak, J. M., Schmuki, P., & Krýsa, J. (2007). Electrochemically assisted photocatalysis on self-organized TiO2 nanotubes. *Electrochemistry Communications*, *9*(12), 2822–2826. https://doi.org/10.1016/j.elecom.2007.10.002